Available online at www.sciencedirect.com

SciVerse ScienceDirect

Journal of the European Ceramic Society 32 (2012) 1541–1549

www.elsevier.com/locate/jeurceramsoc

Revealing crack profiles in polycrystalline tetragonal zirconia by ageing

F.G. Marro [a,b,*], E. Camposilvan [a], M. Anglada [a,b]

[a] Dept. of Materials Science and Metallurgical Engineering, Universitat Politècnica de Catalunya, Av. Diagonal 647, 08028 Barcelona, Spain
[b] Center for Research in Nanoengineering, CRnE, Universitat Politècnica de Catalunya, Pascual i, Vila 15, 08028 Barcelona, Spain

Received 15 September 2011; received in revised form 13 December 2011; accepted 11 January 2012
Available online 22 February 2012

Abstract

Exposure to hot water vapour is shown to be useful for staining indentation crack profiles in doped zirconia polycrystals. This is illustrated here in 3Y-TZP with two different grain sizes, for which Vickers indentation cracks are of Palmqvist type, as well as in 3Y-TZP with 2.5 wt.% cerium oxide, for which indentation cracks are half-penny. The crack profile is clearly revealed on the fracture surface after biaxial flexural testing in all the specimens previously exposed to hot water vapour. The contrast in 3Y-TZP is induced by t–m transformation caused by hydrothermal degradation, which induces an intergranular fracture zone in front of the initial position of the indentation crack tip. The biaxial strength and apparent fracture toughness of 3Y-TZP increase substantially with the time of exposure at a rate that depends on the grain size. On the contrary, in 3Y-TZP doped with ceria no signal of t–m transformation is found and the flexure biaxial stress remains practically constant, but the initial position of the indentation crack is also clearly revealed by an intergranular fracture zone in front of the initial position of the crack tip. In this case, this is associated to environmentally assisted slow crack growth under the indentation residual stress during exposure to hot water vapour in autoclave.

Keywords: Fracture; Optical microscopy; Mechanical properties; Strength; ZrO_2

1. Introduction

Indentation cracks have been frequently used to study the fracture toughness of ceramics either from the measurement of their crack length or from strength testing of indented specimens (surface crack in flexure methods).[1] In such strength tests, it is essential either to have an exact knowledge of the indentation residual stresses or otherwise make sure they are removed by polishing or annealing the indented specimen before testing. This requires knowledge of the starting crack for a posterior fracture mechanics analysis, but the crack profile is frequently difficult to visualize during the post-mortem fractographic examination due to poor visual contrast. Environmentally assisted slow crack growth may also be present during indentation or when the stress is raised in strength testing at room temperature, and this opens the question of the actual crack dimensions that have to be considered in the calculations. Swab and Quinn[2] studied in 1998 the fracture surfaces of different indentation pre-cracked ceramics after strength testing at room temperature showing the presence of what they called "halos" around the periphery of indentation cracks. In many of their ceramics, this halo was attributed to environmentally assisted slow crack growth (in alumina and glass) or to the indentation-induced residual stresses which initiated crack growth.

In polycrystalline tetragonal zirconia stabilized with 3% molar yttria (3Y-TZP) it is not easy to identify the initial crack shape on the fracture surface of an indented pre-cracked specimen. Halos around indentation cracks are not usually observed for this ceramic in spite of possessing substantial slow crack growth behaviour at room temperature.[3] Susceptibility to hydrothermal ageing is a distinctive feature of 3Y-TZP[4–8] that is, the formation of monoclinic content at the surface during exposure to humid environments. The kinetics of ageing in air is maximal around 250 °C and there is evidence that ageing is also operative at much lower temperatures.[5,8] Hydrothermally aged 3Y-TZP specimens presents a micro-cracked surface layer whose thickness increases with ageing time whilst the flexural strength decreases after long ageing times. If the ageing conditions are aggressive enough, the specimen can even disintegrate. For example, Boukis et al.[9] investigated the corrosion

* Corresponding author at: Center for Research in Nanoengineering, CRnE, Universitat Politècnica de Catalunya, Pascual i, Vila 15, 08028 Barcelona, Spain. Tel.: +34 93 40 54454.
E-mail address: fernando.garcia.marro@upc.edu (F.G. Marro).

0955-2219/$ – see front matter © 2012 Elsevier Ltd. All rights reserved.
doi:10.1016/j.jeurceramsoc.2012.01.013

resistance of Y-TZP in simulated supercritical water oxidation environment at 465 °C and at the pressure of 25 MPa. Under these severe conditions, the ceramic just disintegrated. Under less severe conditions, Kojima et al.[10] also found that 3Y-TZP sintered at temperatures equal or higher than 1550 °C disintegrated under ageing in a range between 200 °C and 400 °C and at a pressure of 30 MPa. The degree of disintegration depended on the grain size of the sintered body and the ageing temperature.

If an indentation crack in 3Y-TZP is exposed to water vapour, it is expected that the exposed crack surfaces will transform to monoclinic phase in a similar way as the specimen surface. As this ageing process is normally accompanied of micro-cracking, the aged crack tip will become visible on the fracture surface as a zone showing the typical morphology of degraded surface layers with intergranular fracture if adequate degradation conditions are used. Recently, we have observed[11] a strong contrast on the fracture surface in the periphery of the indentation crack in commercial 3Y-TZP subjected to ageing. That work focused on the changes in the fracture strength that were detected in indented specimens after long ageing times. Here we focus on the visual contrast produced by the water vapour exposure in the periphery of indentation cracks in 3Y-TZP ceramics with different susceptibilities to hydrothermal degradation. The effect of water vapour is also investigated in another yttria doped zirconia ceramic that was made stable in front of hydrothermal degradation by the addition of cerium oxide. Although in this ceramic no t–m transformation was expected in front of the crack tip, the crack front could be detected by the marks left on the fracture surface by environmentally assisted slow crack growth during exposure to water vapour.

The present work focuses on using ageing as a method for "staining" the crack profile so that it can be observed easily by fractography. This method can be used in sacrifice indented and annealed specimens to properly identify the crack profile, and then the strength can be measured in identical indented and annealed but non-degraded specimens. In this way, one can obtain the fracture toughness without uncertainties about the effect of hydrothermal ageing on the strength. However, the method might be also used to mark the crack profile in the actual specimens tested for the determination of fracture toughness, as far as it may be proved that degradation for short times has a negligible influence on the strength.

2. Materials and methods

Commercial TZ-3YSB-E powder (Tosoh Co., Japan) was cold isostatic pressed at 200 MPa producing green compact bars which were sintered in an alumina tube furnace (Hobersal ST-18) with heating and cooling rates of 3 °C/min. Two sintering temperatures were used: 1450 °C and 1550 °C; producing two materials with different grain size (named here as AS5 and AS7, respectively). A third material (AS3) was produced from the same starting powder (TZ-3YSB-E) by presintering at 1200 °C producing a bar with ∼35% apparent porosity as measured by mercury intrusion porosimetry. The porous bar was cut into discs of 2 mm thickness, which were then immersed in a solution of 50% by weight of a cerium salt solution in ethanol (Alfa Aesar Cerium III Nitrate Hexahydrate). After immersion of the discs for 10 min, they were dried at 200 °C for 1 h and then sintered at 1450 °C for 2 h to achieve full density. The final specimens produced in this way contained 2.5% wt cerium on their surface as analysed by Electron Probe Micro Analysis (EPMA Cameca sx50). AS3 possessed a similar grain size as AS5 but lower t–m phase transformability at the surface. CeO_2 is a stabilizer of the tetragonal phase, inducing a lower fracture toughness and decreasing the susceptibility to ageing due to its higher phase stability. The reason to choose AS3 was to study the effect of hydrothermal exposure on the indentation crack when no ageing occurs. As AS3, AS5 and AS7 possessed different fracture toughness and crack shapes, the influence of these parameters on the resistance to hydrothermal degradation can be assessed. The numbers 3, 5 and 7 next to AS indicate the value of the indentation fracture toughness of each material.

Indentation fracture toughness in air, K_{IC}, was determined with the aim of ranking the materials in terms of fracture toughness. Vickers indentations were done at 5, 10, 20 and 40 kg and the produced cracks were used to estimate K_{IC}. For AS5 and AS7, the cracks were of Palmqvist type (not connected below the imprint) and K_{IC} was determined with the equation proposed by Niihara et al.[12]:

$$K_{IC} = 0.025\left(\frac{E}{H}\right)^{0.4}\left(\frac{PH}{8c}\right)^{1/2}; \quad 1 \le \frac{2c}{d} \le 2.5 \tag{1}$$

where d is the imprint semi-diagonal, $2c$ the observed crack length at the surface (distance from imprint corner to crack tip), E is the Young modulus, and the hardness parameter stands for $H = P/2d^2$ (P is the indentation load). For AS5 it was obtained $K_{IC} = 5.1 \pm 0.1\ \text{MPa m}^{1/2}$, whilst the coarse-grained material AS7 showed a higher fracture toughness of $K_{IC} = 6.9 \pm 0.2\ \text{MPa m}^{1/2}$. For AS3, the indentation cracks were connected below the imprint and K_{IC} in this case was determined with the equation proposed by Anstis et al.[13]:

$$K_{IC} = 0.016\left(\frac{E}{H}\right)^{0.5} Pc^{-3/2} \tag{2}$$

Here c represents here the radius of the half-penny crack. For AS3, it was then obtained that $K_{IC} = 2.9 \pm 0.1\ \text{MPa m}^{1/2}$ ($3.8 \pm 0.1\ \text{MPa m}^{1/2}$, in case Niihara equation is used). Although indentation methods give only rough estimations of the actual fracture toughness,[14] it is clear that fracture toughness increases in the order AS3, AS5 and AS7. From the sintered bodies, discs were obtained with 10 mm diameter and 2 mm thickness, which were polished up to colloidal silica finishing achieving an average roughness of $R_a \le 0.005\ \mu\text{m}$. The Young modulus was 230 GPa for all materials as measured by the impulse excitation technique (GrindoSonic MK5i) and the bulk density was over 99% of the theoretical full density as determined by the Archimedes method. The rest of mechanical properties are given in Table 1. All materials had a fully tetragonal microstructure; however, the existence of a small amount of cubic phase cannot be ruled out because of the overlapping of the cubic and tetragonal phases.

Table 1
Properties of the materials: final sintering conditions (temperature and time), average grain size, 1 kg Vickers hardness, indentation fracture toughness K_{IC} and monoclinic content at the surface after 100 h of exposure in autoclave.

Material	Sintering	Grain size (μm)	HV1 (GPa)	K_{IC} (MPa m$^{1/2}$)	V_m
AS3	1450 °C, 2 h	0.30	12.0	2.9	0%
AS5	1450 °C, 2 h	0.30	12.0	5.1	80%
AS7	1550 °C, 4 h	0.85	16.0	6.9	80%

The specimens were indented at the centre with a 10 kg load, producing Palmqvist cracks at the imprint corners in AS5 and AS7, but in AS3 they were half-penny cracks as previously mentioned. The strength of the specimens was controlled by these cracks, since they were much larger than the critical defect size of non-indented specimens. In order to remove the indentation residual stresses, only AS5 specimens were annealed at 1200 °C for 1 h after indentation. Afterwards, the specimens were hydrothermally aged by exposure to 100% steam atmosphere in autoclave at 131 °C and 2 bar pressure for different times up to 100 h. AS3 and AS7 indented specimens were also hydrothermally aged under the same conditions, but without previous annealing. In order to determine the monoclinic content at the surface of the specimens, X-ray diffraction (XRD) was performed on the aged discs with Cu K_α incident radiation (1.5406 Å) in symmetric θ–2θ configuration with a Bruker AXS D8 diffractometer. From the XRD spectra, the monoclinic volume fraction was then determined as[15]:

$$V_m = \frac{1.311(I_m(\bar{1}\,1\,1) + I_m(1\,1\,1))}{1.311(I_m I_m(1\,1\,1)) + I_t(1\,0\,1)} \quad (3)$$

Here I_t and I_m represent the integrated intensities of (1 1 1) tetragonal and of either ($\bar{1}$ 1 1) or (1 1 1) monoclinic peaks, respectively. To study the effect of water vapour exposure on the strength of the indented discs, these were broken by a ball-on-three ball test in an Instron 8511 machine with WC balls of 6 mm diameter at 20 N/s loading rate. For this biaxial flexural test, the stresses in the disc centre have been previously determined by finite element analysis by Börger et al.[16,17] The maximum stress at the disc centre can be obtained from the following expression[18]:

$$\sigma_{\max} = \frac{3F}{4\pi t^2}\left[2(1+\upsilon)\ln\left(\frac{R}{\alpha t}\right) + (1-\upsilon)\left(\frac{R}{R_D}\right)^2\right] \quad (4)$$

where F is the applied load, υ is the Poisson's ratio of the material taken here as 0.3, R_D and t are the disc radius and thickness, respectively, and R is the support radius (distance from the disc centre to the support points). The parameter α ensures an equi-biaxial stress state in the specimen centre; a value of $\alpha = 0.2$ was suggested by Fett et al.[18] from FE-results reported by Shetty et al.[19] for $R/R_D = 0.75$, $\upsilon = 0.3$, and $t/R_D = 0.1$. The fracture surfaces of the broken disc specimens were observed by laser scanning confocal microscopy (LSCM, Olympus Lext) and then by scanning electron microscopy (SEM, JEOL JSM 6400). Focused ion beam (Zeiss Neon 40 FIB/SEM crossbeam) was used to mill cross-sections and visualize the microstructure around a crack after exposure to water vapour.

Fig. 1 shows the top view of two indented AS5 specimens; one is an indented disc showing the produced indentation cracks, the other image shows a portion of an indented disc just after fracture by the biaxial flexural test. All indented discs fractured into two half-pieces, and in this figure it can be appreciated how the fracture plane corresponds to indentation in one indentation crack plane, thus enabling their posterior visualization as appreciated in the following images).

3. Results

As a consequence of their different grain size and stabilizer content, the materials studied showed different susceptibility to hydrothermal ageing. This was evaluated considering the growth rate of the degraded layer on the surface of the specimen, as observed in cross-section from the fracture surfaces of broken specimens. This layer is known to be rich in monoclinic content due to the water-induced t–m transformation; however, it does not exactly correspond to the monoclinic content profile[20]; it rather indicates the depth of the specimen up to which the structural integrity has been affected by the water species so that the fracture mode becomes completely intergranular.

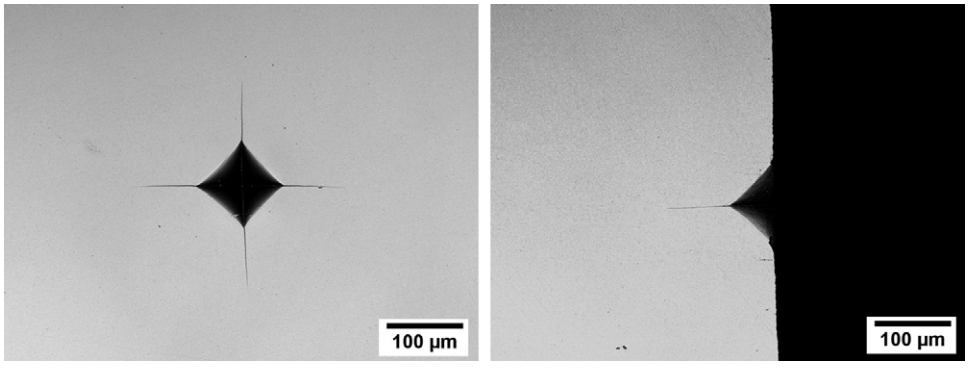

Fig. 1. LSCF micrographs showing an indentation on two AS5 specimens: (left) top view of a disc just after indentation (right) top view of an indented disc after fracture by biaxial test.

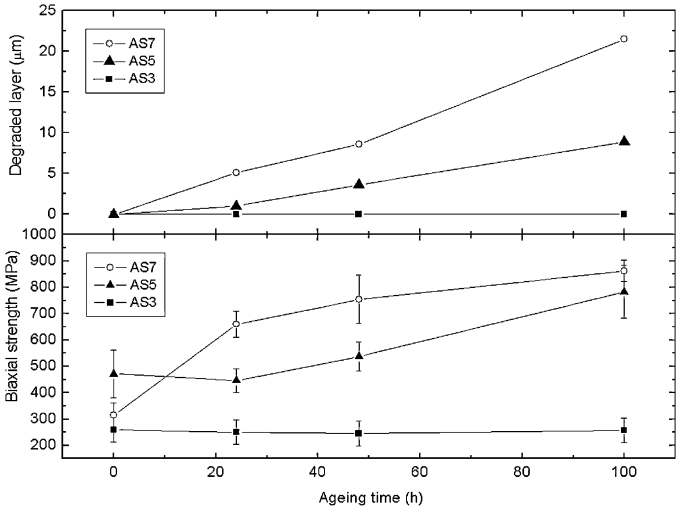

Fig. 2. Change with ageing time of the surface degraded layer and the biaxial strength for 3Y-TZP specimens with a 10 kg indentation. The evolution of both parameters with ageing time is shown for the three different 3Y-TZP conditions (AS3, AS5 and AS7). This layer corresponds to the intergranular zone that can be appreciated on the fracture surface of an aged specimen.

Fig. 2 shows the growth of the surface degraded layer with ageing time for the different material conditions. Low-toughness AS3 was resistant to ageing even after 100 h of hydrothermal exposure, as revealed by the lack of degraded layer on the fracture surfaces. Characterization by XRD showed no monoclinic phase content on the AS3 specimens after the longest hydrothermal exposure. On the other hand, AS5 (which corresponds to the standard grade 3Y-TZP) was susceptible to ageing, showing a growth of the surface degraded layer up to 9 μm after 100 h of hydrothermal exposure. After this long time, the monoclinic content was up to 80% on the surface of the specimens as determined by XRD. Finally, AS7 was the most susceptible to ageing, presenting a degraded layer of about 20 μm after 100 h of hydrothermal exposure. As explained before, AS7, which has the coarser grain size, was also the most degraded, due to the well established relationship between transformability and grain size.[4,21–23]

Fig. 2 also shows the evolution of the biaxial strength of the indented specimens with the time of exposure in autoclave. For AS3, the initial strength of indented specimens before autoclaving was around 260 ± 50 MPa, and it remained the same even was after the longest exposure to autoclave. The strength of AS3 was the lowest as compared to AS5 and AS7, which is related to its lower fracture toughness and to the indentation crack geometry (as shown in Figs. 3–5). The indented and annealed AS5 specimens had an initial strength (without autoclaving) of 470 ± 90 MPa. It should be outlined here again that these specimens were annealed at 1200 °C in order to remove any indentation residual stress. No change in the strength was found in AS5 after only a few hours of autoclaving, however, after 48 h the strength began to increase substantially. Indeed, after 100 h it had increased up to 700 MPa. This increase in strength of indented specimens with ageing cannot be explained by relaxation of the indentation residual stresses by ageing, as these were initially removed by annealing as mentioned previously. The reason for this strength increase in AS5 has been addressed elsewhere.[11] It can be seen that the effect is even stronger in AS7 indented specimens whose strength is more than 700 MPa only after a few hours of autoclaving. However, for ageing periods longer than 50 h, the strength of AS7 practically did not increase any further as can be appreciated in Fig. 2.

Strengthening on zirconia-based ceramics by residual stresses created by transformation is a well-known phenomenon in zirconia-based laminates[25,26] in which the strengthening is due to compressive residual stresses in the external transformed layer induced during cooling from the sintering temperature. However, the strengthening described here is related to large indentation cracks nearly an order of magnitude deeper than the thickness of the surface transformed layer. The transformed layer has hardly any effect on the flexure strength of degraded smooth specimens after short ageing times, whilst reduces significantly the strength after long ageing times.[27] The fracture surfaces of the indented discs subjected to hydrothermal treatment were visualized by SEM. This allowed confirmation of previous findings in non-annealed AS5,[11] where it was observed that the edge of the indentation cracks becomes marked if the indented specimen had been hydrothermally exposed. For AS3 a bright and wide "halo" could be clearly observed around the periphery of the indentation crack (Fig. 3). Close inspection reveals that this halo corresponds to a zone of intergranular fracture; however, no degraded layer appears close to the surface of the discs outside the indentation region. This absence of degraded layer is coherent with the fact that the AS3 condition is resistant to ageing. In this low-toughness material, the revealed cracks are half-penny type (connected below the imprint), and the crack depth is about 145 μm.

The fracture surface of the indented, annealed and aged AS5 specimens also presents a bright contrast around the edge of the indentation crack as observed by SEM (Fig. 4). It can also be appreciated that AS5 is susceptible to hydrothermal degradation by the presence of the degraded layer with intergranular fracture close to the surface of the discs (outside the indentation region). Close inspection of the contrasted region in front of the indentation crack edge reveals again that the fracture is intergranular. In this higher toughness material condition, the cracks induced by the indentation can be appreciated to be of Palmqvist type (not connected below the imprint) with a depth of 73 μm. Finally, the fracture surface of the AS7 specimens (Fig. 5) clearly manifests their higher toughness by the smaller size of the indentation cracks, which are also of Palmqvist type and with a depth of only 44 μm. This material was the most susceptible to degradation showing the largest degraded layer at the surface.

Fig. 6 displays the fracture surfaces of indented AS5 specimens subjected to different ageing times, as observed by LSCM microscopy. This figure demonstrates that optical microscopy is sufficient in order to appreciate the contrast around the edge of the crack. If the indented specimens are not autoclaved, then their fracture surfaces show practically no contrast, being difficult to determine the initial indentation crack profile (Fig. 6a). After 24 h of autoclave, a thin dark zone can be appreciated in front of the crack edge similar to that found near the surface of

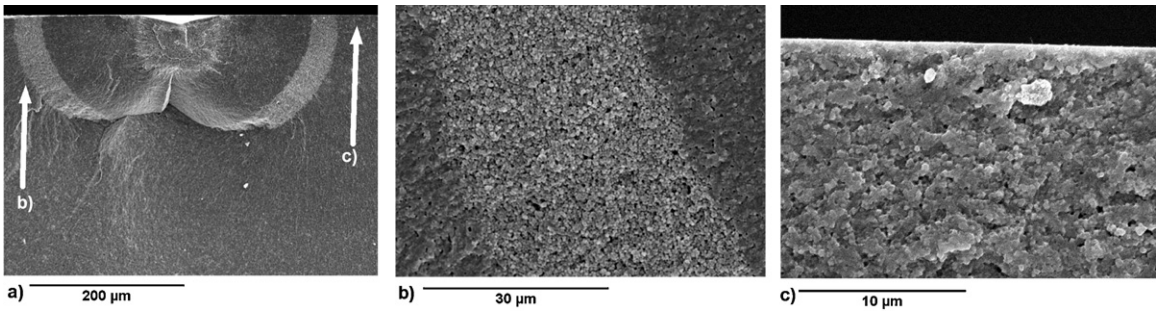

Fig. 3. SEM micrographs showing the fracture surface of an indented (10 kg) AS3 specimen exposed for 100 h to water vapour in autoclave: (a) general view, (b) detail of the periphery of the crack, and (c) detail of the surface of the specimen.

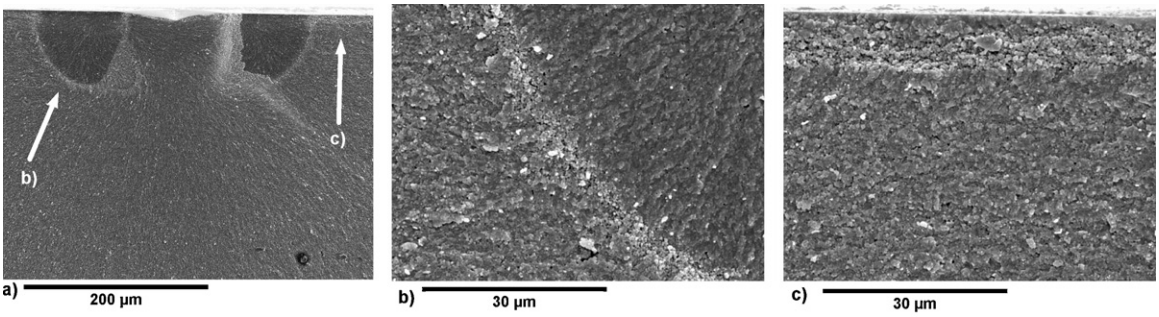

Fig. 4. SEM micrographs showing the fracture surface of an indented (10 kg) AS5 specimen exposed for 100 h to water vapour in autoclave: (a) general view, (b) detail of the periphery of the crack, and (c) detail of the surface of the specimen.

the specimen as a consequence of the action of water. It corresponds to the bright contrast that can be appreciated by SEM. Its different appearance by using the two different microscopy techniques is because they produce different contrast on the same area: in SEM, an intergranular fracture zone of a non-conducting specimen appears in brighter contrast due to electrical charging of the surface at that location, whilst in optical microscopy the same zone appears as dark since a higher roughness surface is less reflective to light. For longer exposures to autoclave (48 h and 100 h), both the dark zone around the crack edge and the degraded layer on the surface of the discs increase. These images show that only 24 h of exposure to water vapour in autoclave is sufficient in AS5 to clearly reveal indentation cracks on the fracture surface of standard 3Y-TZP, as examined simply by optical microscopy.

It is worth to outline that the AS3 specimens were resistant to ageing so that water vapour did not induce any t–m transformation on the edge of indentation cracks. However, the dimensions of the indentation crack increased during autoclaving. It was actually observed that the 10 kg indentation crack increased its length from 110 µm to about 150 µm after the hydrothermal exposure. Inspection by Atomic Force Microscopy (AFM) of the extended crack showed a marked intergranular path, suggesting subcritical crack growth induced by the hydrothermal exposure (Fig. 7). Therefore, environmentally assisted slow crack growth occurs in AS3 during hydrothermal exposure without any detectable t–m transformation.

Inspection of the indentation crack below the degraded surface layer of the discs was performed on an indented AS5 specimen by means of Focussed Ion Beam (FIB) milling. After autoclaving for 100 h, the surface was ground and polished in order to remove completely the surface degraded layer of the discs and the crack was observed from the top (Fig. 8a). FIB

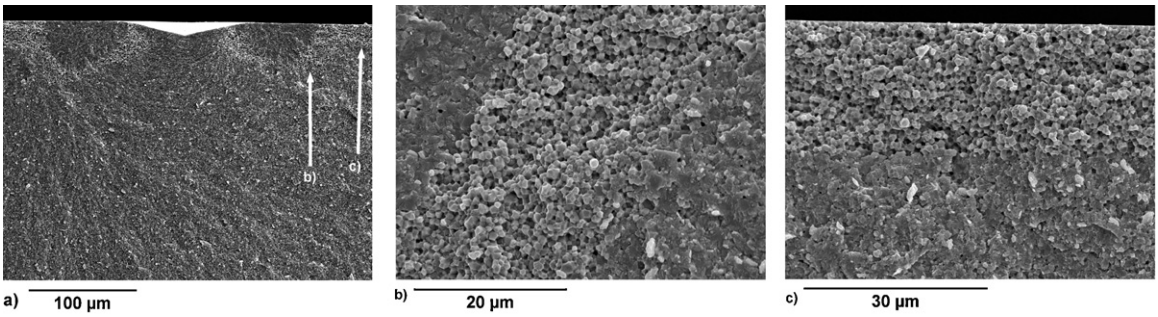

Fig. 5. SEM micrographs showing the fracture surface of an indented (10 kg) AS7 specimen exposed for 100 h to water vapour in autoclave: (a) general view, (b) detail of the periphery of the crack, and (c) detail of the surface of the specimen.

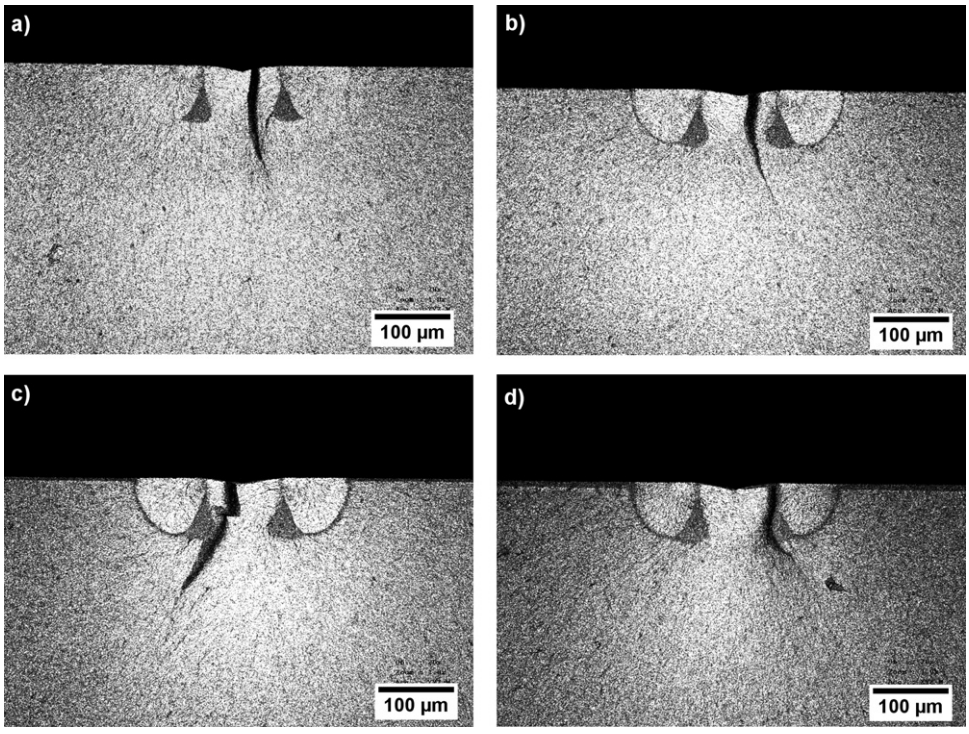

Fig. 6. LSCF micrographs showing the fracture surfaces of indented (10 kg) AS5 specimens exposed to water vapour in autoclave for different periods of time: (a) no ageing, (b) 24 h, (c) 48 h, and (d) 100 h.

milling was used to produce a trench on the crack (Fig. 8b), and the cross-section was then polished by ion beam milling allowing the evaluation of the material at both crack faces. The crack is almost completely closed and its trace into the bulk can be barely detected (Fig. 8c), in part because the cross section selected is very close to the crack tip and also because of the expansion related to transformation by effect of water vapour. It can also be appreciated that the material on both crack faces is highly micro-cracked. This micro-cracking is typical of the affected layer of degraded 3Y-TZP,[4,11,24] proving that the water vapour reached indeed the crack tip producing the spontaneous t–m transformation process.

4. Discussion

The initial indentation crack profile could hardly be discerned on the fracture surfaces of specimens tested in flexure (Fig. 6a). However, if the specimens were exposed to water vapour in autoclave before testing, then the border of the indentation crack was clearly resolved on the fracture surface. This procedure may

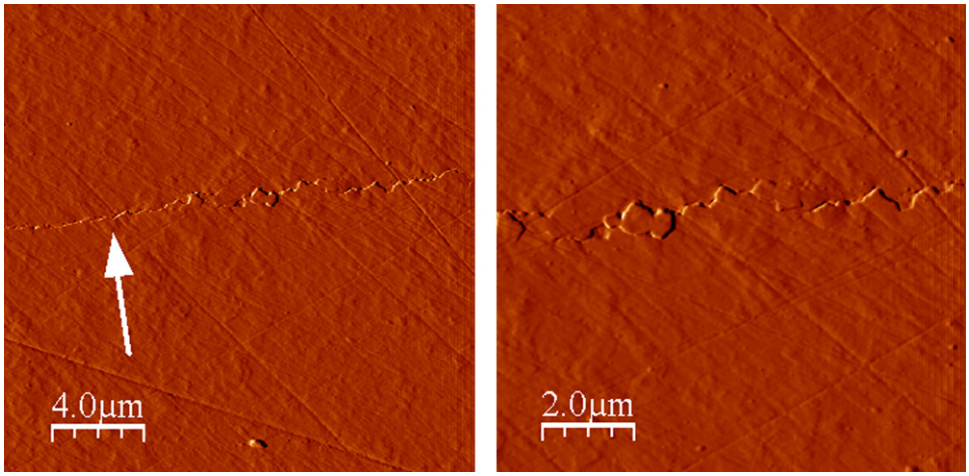

Fig. 7. Atomic Force Microscopy (AFM) images of a 10 kg indentation crack on an AS3 specimen after 100 h exposure to water vapour. The arrow in the left micrograph indicates the beginning of the assisted slow crack growth during autoclaving; the other micrograph clearly reveals the irregular path of the extended crack.

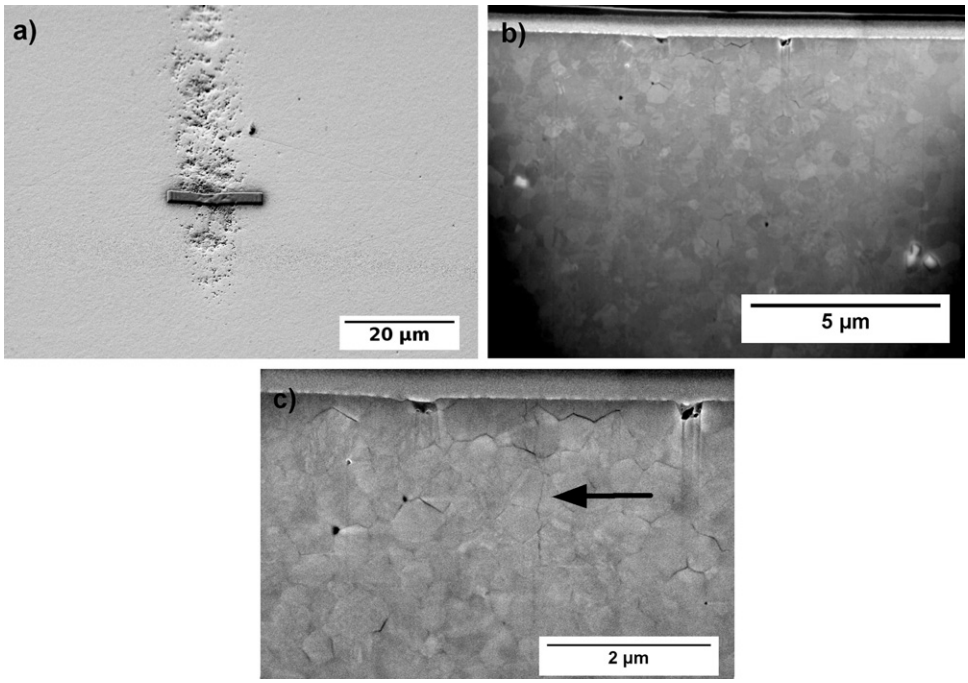

Fig. 8. FIB cross-section of a 10 kg indentation crack on an AS5 specimen degraded for 100 h. The specimen was grounded and polished after ageing in order to remove the surface degraded layer: (a) top view of the degraded crack after grinding and polishing the specimen surface (the platinum layer indicates the location where the FIB trench was milled), (b) general view of the produced FIB trench, and (c) closer view of the polished trench, showing microcracks present around the crack (crack path is indicated by an arrow).

be used as a simple method to mark the edge of indentation cracks in TZP zirconia.

4.1. Effect of water on AS3

The origin of the observed intergranular fracture region around the indentation crack in AS3 is different than for AS5 and AS7. AS3 is not susceptible to ageing, so that during autoclaving no t–m transformation took place as determined by XRD. However, the indentation crack in these specimens increased during autoclaving as observed from the crack length on the specimen surface. The original crack profile and the ensuing extension by subcritical crack growth are clearly revealed on the fracture surfaces as an intergranular fracture zone. In spite of such crack growth by hydrothermal exposure, the strength of indented AS3 specimens was not affected. This can be explained by noting that the residual stress intensity factor can be written in terms of crack length as[28]:

$$K_r(t) = K_{IC}\left(\frac{c_o}{c(t)}\right)^{3/2} \quad (5)$$

where c_0 is the initial indentation crack length in an inert environment and $c(t)$ is the crack length after subcritical crack growth in contact with water vapour for a time t. The dependence between crack velocity, dc/dt, and stress intensity factor (SIF), K, is usually represented by a power law, that is,

$$\frac{dc}{dt} = v_0\left(\frac{K}{K_{IC}}\right)^n \quad (6)$$

where v_0 and n are constants. This behaviour is obeyed in the three stages of subcritical crack growth, with different values of n and v_0 at each stage.[3] Crack growth is fastest immediately after indenting when $K \approx K_{IC}$, and decreases rapidly as soon as $K < K_{IC}$ since the exponent n is usually very high (normally >15). The crack growth will stop when K reaches the threshold for environmental subcritical crack growth, K_{Ith}. The crack extension that takes place in the autoclave is relatively large since, after 100 h, c is about 36% longer than c_0, and this implies a reduction to about 63% of the initial residual SIF. As the SIF threshold is about 57% of K_{IC} for 3Y-TZP,[3] this means that the indentation crack could still grow, but at lower rate, if the disc was left longer in the autoclave. Therefore, the increase in crack length after hydrothermal ageing is compensated by a reduction in the residual SIF so that the strength is kept constant. The strength of indented specimens in unidirectional flexure tests depends only of the indentation load and does not depend on the amount of crack environmental slow crack growth that may take place during the time elapsed after indentation until strength testing. On the other hand, the lower strength of AS3 in the only indented condition with respect to AS5 and AS7 in the same condition is related to its lower fracture toughness.

4.2. Effect of water on AS5 and AS7

In AS5 and AS7, exposure to water vapour induces t–m phase transformation on the exposed surface forming a degraded layer (Figs. 4c and 5c) with high monoclinic content as confirmed by XRD (Table 1). The profile of the Palmqvist indentation cracks in AS5 and AS7 is revealed after ageing, showing different

crack shapes for both conditions. The crack edges undergo t–m phase transformation during hydrothermal exposure (as clearly revealed by FIB cross-section) and the transformed zone in front of the crack increases with ageing time. This is in agreement with the progression of the t–m transformation underneath any surface during autoclaving. Since AS7 is more transformable, the contrasted region in front of the crack tip is larger than in AS5. The same behaviour is found for the thickness of the degraded layer on the surface of the discs, which grows faster in AS7 than in AS5. This shows that the main variable that explains the difference between AS5 and AS7 is their different t–m transformability rather than the presence of indentation residual tensile stresses.

The strengthening of indented 3Y-TZP with ageing can be explained by crack tip blunting. The formation of the micro-cracks in front of the crack tip may be aided by the tensile residual indentation stresses. This region will be subjected to triaxial stresses by the indentation residual stress field as well as by applied stress during strength testing. The existing micro-cracks may then extend and coalesce with other microcracks given rise to intergranular fracture and some grain may be detached and produce debris in front of the crack tip on the fracture surface (see Fig. 5). The crack will extend until encountering the high toughness tetragonal bulk only a few microns ahead. In this process, the tip effective radius increases proportionally to the thickness of the degraded zone. Strengthening will take place only when the radius of the crack tip becomes larger than a minimum value; so that some degradation time will be needed before the phenomenon appears. This time will be shorter for AS7 since it is more susceptible to ageing.

It may be appealing to explain the increase in strength after autoclaving in AS5 and AS7 by transformation toughening instead of crack tip blunting. It is clear that compressive residual stresses appear on the transformed zones (both on the surface degraded layer as well as near the crack edge). But there are some differences with respect to transformation toughening. In transformation toughening the transformed zone in front of the crack is not micro-cracked, and, in principle, its effect on crack growth resistance is effective as the crack extends (R-curve). By contrast, we assume here that the water species transform and micro-crack the region adjacent to the crack tip without any crack growth, so that when the specimens are tested in biaxial flexure the cracks in this region coalesce inducing a blunted crack in front of the high toughness tetragonal phase. This is supported by the debris that appears on the fracture surface at the original indentation crack profile.

4.3. Fracture toughness

The stresses in the B3B test are not symmetric with respect to the disc centre, but the symmetric stress solution for the ball-on-disc test given in Eq. (4) describes also the stress state in this non-symmetric case with deviations less than 5% for $x/R_D < 0.15$ as shown by Fett et al.[18] As the discs were indented at the centre with a 10 kg load, both types of indentation cracks studied here extended from the centre up to distances lower than 5% of the disc radius. Hence, the stress on the indentation crack in the ball on three balls testing device used here is practically constant and equal to the maximum stress given by Eq. (5). Fett et al.[18] also concluded that tensile stresses in the depth direction in the centre of the disc diminish linearly until zero at half the thickness. The mode I stress intensity factor at fracture can then be written as,[29]

$$K_{IC} = f\left(\frac{a}{t}\right)\sigma_{\max}\sqrt{t} \tag{7}$$

The function $f(a/t)$ depends on the ratio of the elliptical crack semi-axis a/c and is only available for $a \leq c$. We now compare the present results for strength with those for fracture toughness of AS5 since for these specimens the SFI of the indentation crack is only the applied stress as the indentation residual stress had been removed by annealing after indentation. For simplicity, we shall consider the values provided for this function when $a = c$ (semi-circular crack); and the crack size was measured on the fracture surface of the specimen after ageing for 24 h ($a = 73\ \mu m$). For the present disc thickness ($t = 1.9$ mm), we have $f(a/t) \approx 0.24$. By using the strength of the non-degraded specimen (see Fig. 2) we can calculate the fracture toughness by using Eq. (7) obtaining $\approx 4.9\ MPa\ m^{1/2}$, which is a reasonable value in the range of values often measured in biomedical grade 3Y-TZP by using normalised standard fracture mechanics tests methods in pure mode I. This demonstrates that if the ageing time used for marking the crack is short enough so that strength is not affected (as here for 24 h ageing in AS5 material), then the observed final strength and the marked crack dimensions can be both used directly in the final fracture mechanics evaluation. However, one should be sure the crack is not blunted by ageing since Eq. (7) does not hold for a blunted crack. If the time of ageing is long (for example, like here 100 h autoclave in AS5), then the strength obtained is 783 ± 90 MPa, without any significant change in the crack length or shape ($f(a/t)$ does hardly change with ageing). The measured fracture toughness would then be affected by the radius of the degraded microcracked zone that has been transformed by the effect of the water vapour, which now is of about 5 μm (Fig. 8).

The increase in volume associated to t–m transformation does not produce an important increase in shielding since transformation is starting always on the surface, that is, on the crack faces directly and not in front of the crack tip as in transformation toughening. This may explain why there is no increase in strength is after 24 h of ageing and the very small increase after 48 h.

For AS5, short ageing times do not affect the strength, the fracture toughness can be determined in specimens previously aged in order to reveal the crack shape and dimensions. In this case, the width of the degraded zone in front of the crack tip after 24 h ageing is of about 1 μm, so that the crack is still sharp enough for using Eq. (7). In general, the minimum ageing time necessary to keep the sharp crack enough (and therefore do not affect the strength) for an indented specimen will depend on the degree of degradation of the crack tip. In AS7 the grain is coarser than in AS5, therefore ageing is faster, so that a shorter ageing time is needed in AS7 to stain the crack edge without affecting the strength of indented specimens.

5. Conclusions

The main conclusions are summarized as follows:

- Exposure to hot water vapour is useful for revealing the profiles of indentation cracks in tetragonal polycrystalline zirconia. The procedure was illustrated in 3Y-TZP specimens of different grain size with Palmqvist indentation cracks of different shape. The crack profile is clearly revealed on the fracture surfaces after flexural testing if the specimens are previously exposed to 131 °C water vapour in autoclave. The contrast is produced by intergranular fracture in a region in front of the initial position of the crack tip which is induced by tetragonal-to-monoclinic phase transformation during the water vapour exposure. After long ageing times, the biaxial strength and corresponding apparent fracture toughness increase substantially.
- 3Y-TZP doped with 2.5% weight ceria by infiltration in the presintered state, is resistant to hydrothermal degradation, less tough and indentation cracks are median. But the initial indentation crack profile is also clearly revealed which is associated to the existence of strong environmentally assisted slow crack growth under indentation residual stress during autoclaving.

Acknowledgements

The authors gratefully acknowledge the financial support from the *Ministerio de Ciencia e Innovación* (*MICINN*) of Spain through project MAT2008-03398 and the research grant given to F.G. Marro. The general financial support to the research group given by the *Generalitat de Catalunya* is also fully acknowledged (2009SGR01285).

References

1. Quinn GD, Gettings RJ, Kübler JJ. Fracture toughness of ceramics by the surface crack in flexure (SCF) method. *Fract Mech Ceram* 1996;**11**:203–18.
2. Swab J, Quinn GD. Effect of crack "halos" on fracture toughness determined by the surface crack in flexure method. *J Am Ceram Soc* 1998;**81**:2261–8.
3. Chevalier J, Olagnon C, Fantozzi G. Subcritical crack propagation in 3Y-TZP ceramics: static and cyclic fatigue. *J Am Ceram Soc* 1999;**82**:3129–38.
4. Chevalier J, Gremillard L, Deville S. Low-temperature degradation of zirconia and implications for biomedical implants. *Annu Rev Mater Res* 2007;**37**:1–32.
5. Kobayashi K, Kuwajima H, Masaki T. Phase change and mechanical properties of ZrO_2–Y_2O_3 solid electrolyte after ageing. *Solid State Ionics* 1980;**3/4**:489–93.
6. Marro FG, Valle J, Mestra A, Anglada M. Surface modification of 3Y-TZP with cerium oxide. *J Eur Ceram Soc* 2011;**31**:331–8.
7. Marro FG, Mestra A, Anglada M. Contact damage in a Ce-TZP/Al_2O_3 nanocomposite. *J Eur Ceram Soc* 2011;**31**:2189–97.
8. Sergo LV. Low temperature degradation ageing of zirconia: a critical review of the relevant aspects in dentistry. *Dent Mater* 2010;**26**:922–8.
9. Boukis N, Claussen N, Ebert K, Janssen R, Schacht M. Corrosion screening tests of high-performance ceramics in supercritical water containing oxygen and hydrochloric acid. *J Eur Ceram Soc* 1997;**17**:p71.
10. Kojima T, Mori Y, Kamiya M, Sasai R, Itoh H. Disintegration process of yttria-stabilized zirconia ceramics using hydrothermal conditions. *J Mater Sci* 2007;**42**:6056–61.
11. Marro FG, Anglada M. Strengthening of Vickers indented 3Y-TZP by hydrothermal ageing. *J Eur Ceram Soc* 2012;**32**:317–24.
12. Niihara K, Morena R, Hasselman DPH. Evaluation of K_{IC} of brittle solids by the indentation method with low crack-to-indent ratios. *J Mater Sci Lett* 1982;**1**:13–6.
13. Anstis GR, Chantikul P, Lawn BR, Marshall DB. A critical evaluation of indentation techniques for measuring fracture toughness. I. Direct crack measurements. *J Am Ceram Soc* 1981;**64**:533–8.
14. Quinn GD, Bradt RC. On the Vickers indentation fracture toughness test. *J Am Ceram Soc* 2007;**90**:673–80.
15. Toraya H, Yoshimura M, Somiya S. Calibration curve for quantitative analysis of the monoclinic-tetragonal ZrO_2 system by X-ray diffraction. *J Am Ceram Soc* 1984;**67**:C119–21.
16. Börger A, Supancic P, Danzer R. The ball on three balls test for strength testing of brittle discs: stress distribution in the disc. *J Eur Ceram Soc* 2002;**22**:1425–36.
17. Börger A, Supancic P, Danzer R. The ball on three balls test for strength testing of brittle discs. Part II. Analysis of possible errors in the strength determination. *J Eur Ceram Soc* 2004;**24**:2917–28.
18. Fett T, Rizzi G, Esfehanian M, Oberacker R. Simple expressions for the evaluation of stresses in sphere-loaded discs under biaxial flexure. *J Test Eval* 2008;**36**:285–90.
19. Shetty KD, Rosenfield AR, McGuire P, Duckworth WH. Biaxial flexure test for ceramics. *Am Ceram Soc Bull* 1980;**59**:1193–7.
20. Muñoz-Tabares A, Jimenez-Pique E, Anglada M. Subsurface evaluation of hydrothermal degradation of zirconia. *Acta Mater* 2011;**59**:473–84.
21. Watanabe M, Iio S, Fukuura I. Ageing behaviour of Y-TZP. In: Claussen N, Ruhle M, Heuer AH, editors. *Advances in ceramics, vol. 12. Science and technology of zirconia II*. Columbus, OH: The American Ceramic Society, Inc.; 1984. p. 391–8.
22. Lawson S. Environmental degradation of zirconia ceramics. *J Eur Ceram Soc* 1995;**15**:485–502.
23. Gaillard Y, Jimenez-Pique E. Quantification of hydrothermal degradation in zirconia by nanoindentation. *Acta Mater* 2008;**56**:4206–16.
24. Marro FG, Chintapalli R. Study of near surface changes in YTZP after LTD. *Int J Mater Res* 2009;**100**:92–6.
25. Lakshminarayanan R, Shetty DK, Cutler RA. Toughening of layered ceramic composites with residual surface compression. *J Am Ceram Soc* 1996;**79**:79–87.
26. Virkar A, Huang JL, Cutler RA. Strengthening of oxide ceramics by transformation-induced stress. *J Am Ceram Soc* 1987;**70**:164–70.
27. Marro FG, Mestra A, Anglada M. Weibull characterization of the flexural strength of hydrothermally degraded 3Y-TZP zirconia. In: *12th European inter-regional conference on ceramics*. 2010.
28. Lawn B. Fracture of brittle solids. *Cambridge solid state science series*, 2nd ed. Oxford, UK: Cambridge University Press; 1993, 378 p.
29. Schell KG, Fett T, Rizzi G, Esfehanian M, Oberacker R, Hoffmann MJ. *Eng Fract Mech* 2009;**76**:2486–94.